Robotica: (2019) volume 37, pp. 1302–1319. © Cambridge University Press 2019
doi:10.1017/S0263574718001522

Evaluation of Bio-Inspired Scales on Locomotion Performance of Snake-Like Robots

Alexander H. Chang* and Patricio A. Vela

Institute for Robotics and Intelligent Machines (IRIM), School of Electrical and Computer Engineering, Georgia Institute of Technology, Atlanta, GA, USA

(Accepted December 22, 2018. First published online: February 4, 2019)

SUMMARY
The unique frictional properties conferred by snake ventral scales inspired the engineering and fabrication of surrogate mechanisms for a robotic snake. These artificial, biologically inspired scales produce anisotropic body-ground forcing patterns with various locomotion surfaces. The benefits they confer to robotic snake-like locomotion were evaluated in experimental trials employing rectilinear, lateral undulation, and sidewinding gaits over several distinct surface types: carpet, inhomogeneous concrete and homogeneous concrete. Enhanced locomotive performance, with respect to net displacement and heading stability, was consistently measured in scenarios that utilized the engineered scales, over equivalent scenarios where the anisotropic effects of scales were absent.

KEYWORDS: Robotic snake; Scales; Anisotropic forcing; Locomotion; Biomimetic robots.

1. Introduction

Inspired by nature, snake-like robots are expected to assist with tasks like search and rescue, reconnaissance and exploration.[1–5] Through the incorporation of biomimetic design and actuation methods, snake-like robotic systems adopt advantageous locomotive strategies that facilitate mission execution in challenging environments, as demonstrated by their biological counterparts. Mobility in these scenarios requires competent locomotion over a diverse set of terrain, each characterized by distinct body–ground interactions; concrete, pavement, and even carpet exemplify candidate surface types that may be encountered.

Early robotic locomotion experiments on flat surfaces used passive wheels to impose kinematic constraints to enable productive mobility through lateral undulation[6,7] as well as rectilinear motion.[8] Subsequent models demonstrated alternative design strategies, integrating active wheels with passive joints[9] or treads to increase terrain accessibility, as with the OmniTread and KOHGA series of robots.[10,11] Augmentation with additional active mechanisms, however, imposes greater physical footprints and, in turn, more stringent applicability restrictions. These approaches additionally complicate use of shape-based strategies to accomplish other useful tasks such as climbing or rolling.[12–14] Non-wheeled variants of this class of mobile robots exhibit isotropic body–ground forcing profiles. In the presence of large, strategically placed obstacles, lateral undulation is accomplished[15–17] using body-obstacle push-pull principles first uncovered by ref. [18]. Subsequent related efforts have focused on perception-enabled strategies to exploit useful obstacle push points[19,20] as well as body compliance to facilitate obstacle-aided locomotion.[21,22] With respect to clear and flat, open terrain, a kinematic, rolling form of sidewinding arises as the preferred mode of locomotion.[23–26]

* Corresponding author. E-mail: alexander.h.chang@gatech.edu

In contrast to the isotropic body–ground interactions traditionally adopted by serpentine robotic platforms, snake species are known to effect and exploit anisotropic resistance profiles between the body venter (belly) and their locomotion environment. Scales lining the venter generate directionally dependent frictional forcing through interactions with the environment. Specifically, frictional resistance to lateral motion against a surface is greatest compared to that produced during caudal (posteriorly directed) or rostral (anteriorly directed) motion.[27] This characteristic is effectively encoded into the ventral scale morphology at both micro- and macro-scopic levels. Micro-structural patterns in snake ventral scales facilitate greater measured frictional coefficients during lateral versus either caudal or rostral sliding across a surface.[28,29] At the macro-scopic level, scales interact with larger surface protrusions to produce directionally dependent resistance via a ratcheting principle.[30,31]

Analogous morphological augmentations in snake-like robots have produced similar body–ground interactions, predominantly through use of surface- and gait-specific mechanisms. Wheels have long been employed to facilitate lateral undulation.[6,32] A wheel-less variant was engineered to demonstrate the feasibility of exploiting anisotropic body–ground interactions to facilitate this same gait.[33] Active head-tail anchoring[34] as well as passive ratcheting claws[35] are gait-specific strategies that have been applied toward rectilinear forms of locomotion. More direct and generally applicable, biomimetic strategies that transplant the natural anisotropic frictional properties of animal skin have been explored and evaluated, but for legged robotic morphologies.[36]

Operation of snake-like robotic locomotors in intended mission environments generally entails variety in the surface types being traversed as well as diversity in the set of gait options available for use. Integration of biologically inspired scales into a robotic snake presents the opportunity to exploit anisotropic body–ground interactions in order to enhance, and in some cases enable, performance of different gaits over a variety of surface types.

Contribution. Inspired by the natural anatomy of snakes, we engineer artificial, rigid scales into the chassis of a robotic snake in order to confer locomotive advantages comparable to its biological counterparts. The chassis design comprises rigid scales, uniformly distributed across its surface, that collectively generate anisotropic body–ground interactions with several distinct locomotion environments. Least resistance is experienced when sliding the scaled chassis in the rostral direction, across a locomotion surface. Greatest resistance is experienced when sliding laterally, and an intermediate degree of resistance is produced when sliding caudally.

The relative size and morphology of the artificial scales, with respect to asperities that characterize pragmatically selected locomotion environments, do not lend well to traditional methods for characterizing body–ground interactions. Instead, to evaluate the effectiveness of incorporating artificial scales into the exterior of the robotic snake, we characterized their impact on locomotion performance for three different serpentine gaits: traveling wave rectilinear motion, lateral undulation with sinus-lifting and sidewinding. Evaluations were conducted on several obstacle-free terrain types: carpet, inhomogeneous concrete and homogeneous concrete. Locomotion progress of the robotic snake was tracked during comparative scenarios, whereby (1) artificial scales were equipped to the robot and (2) scales were removed and a thick cloth was fitted to the robot, promoting instead isotropic body–ground interactions. Enhanced locomotive performance was measured in all scenarios employing the scaled chassis, relative to their absence.

2. Scale-Augmented Robotic Platform

The robotic snake employed in these experiments extends its predecessor.[37] It has 12 serially connected modules, each consisting of a motor, an aluminum link connecting to the next module and a fabricated plastic chassis encasing both. The chassis exterior is lined with artificial scales on all but one side. The side absent scales is left flat and smooth for the isotropic body–ground interaction experiments. Dynamixel RX-28 servo-motors, manufactured by Robotis, actuate each joint of the robotic snake. A Robotis OpenCM 9.04 microcontroller both supplies power and acts as a serial communication adapter between the motors and a controlling PC. Matlab programs run on the latter, managing execution of locomotion gaits by commanding joint position and velocity trajectories with respect to time. Manually tuned proportional gains, applied to each individual motor, enable adequate tracking of commanded trajectories.

https://doi.org/10.1017/S0263574718001522 Published online by Cambridge University Press

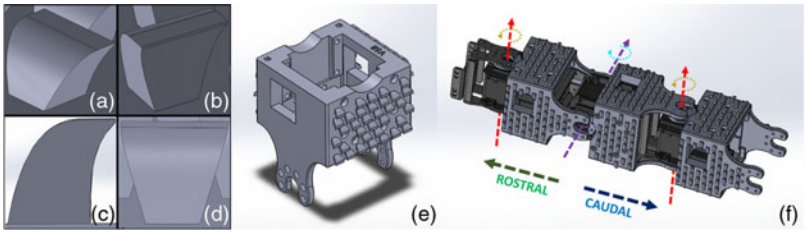

Fig. 1. (a)–(d) Various views of a single scale from the angled rostral face, angled caudal face, lateral face and rostral face, respectively. (e) Scales are located on the surface of each motor chassis. (f) Scaled chassis are integrated into a chain of motors.

2.1. Scaled chassis design

Figure 1 provides a detailed view of an individual scale design. Each scale is 2.75 × 2.5 mm at the base and rises to a height of 3 mm from the chassis surface. The scales on the surface of the chassis interact with locomotion surfaces in a directionally dependent manner, similar to that exhibited by snake skin.[27] The curved, rostral surface of the scale, shown in Fig. 1(a), generates the least amount of resistance when the chassis travels in the rostral direction, along a locomotion surface. From its base, each scale expands to a 5 mm long edge at peak height, in the shape of a caudally oriented hook (Fig. 1(b) and (c)). This feature of the scale promotes greater resistance when the chassis travels in the caudal direction. Additionally, at peak height, each scale forms sharp, laterally oriented hooks (Fig. 1(d)), facilitating the greatest resistance to transverse motion.

The engineered scales are distributed uniformly across three sides of the chassis exterior. They are spaced 6.5 mm apart laterally and 5 mm apart caudal-rostrally along each of these three surfaces. The remaining fourth side is left smooth, with no protruding scales, to aid in comparative testing where the effect of scales must be removed. Figure 1(e) illustrates a CAD rendering of the chassis design. Its base dimensions, absent the scales, are 51 × 51 × 65 mm. A rendering of the scaled chassis, mounted to a series of motors, is illustrated in Fig. 1(f). Adjacent motor axes are separated by a distance of 65 mm. The scaled chassis are oriented with the concave surface (Fig. 1(b)) of the scales facing the caudal end of the robot. All chassis are 3-D printed from Acrylonitrile Butadiene Styrene plastic using a Stratasys Dimension 1200es professional printer, with a precision of 0.33 mm.

Scale geometry was predominantly driven by limitations of the selected fabrication method. Snake ventral scales employ both microscopic and macroscopic features to produce anisotropic forcing profiles with various surfaces. Accessible 3-D print technology admitted reproduction of the macroscopic-level features only to obtain this property. Scale features were sized for comparability with common ground asperities (e.g. those characterizing carpet and concrete). Anticipated wear and tear and printable layer thickness additionally mandated lower bounds on scale dimensions as repeated shearing against rigid surfaces smoothed the original printed scale geometry. Ground asperity distribution patterns influenced the relative scale spacing over the chassis surface.

2.2. Snake robot assembly

Adjacent motors of the robot are arranged such that their axes of rotation are orthogonal to one another, as illustrated in Fig. 1(f). Given a straightened body configuration, every other motor starting from the caudal-most produces yaw actuation while the complementary set of motors produce pitch actuation. The chassis design limits the achievable range of motion to ±65° for each joint.

The entire assembly comprises 11 joints: 5 to produce yaw motion and 6 to produce pitch. Figure 2(a) illustrates the assembled robot snake comprising 12 motors. Each motor, from tail to head, is assigned an ID from 1 through 11, respectively; motor ID 12, seated in the head module, is present only for uniformity. Odd-numbered motors correspond to joints capable of pitch motion (dark-colored modules), while even-numbered motors correspond to those capable of yaw (white-colored modules), similar to the joint numbering scheme employed by ref. [38]. Joints controlling yaw motion are employed to effect shape changes primarily in a horizontal plane, parallel to the locomotion surface. Those controlling pitch are used to lift body segments, vertically, off the locomotion plane. Together, both sets of joints accomplish gait shapes in three dimensions.

https://doi.org/10.1017/S0263574718001522 Published online by Cambridge University Press

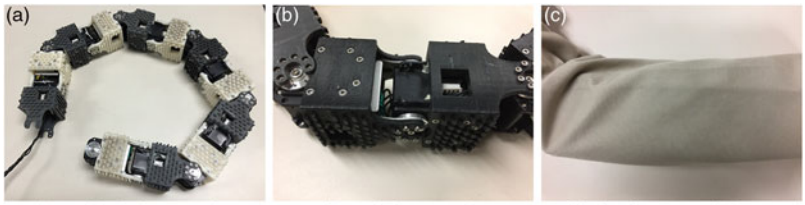

Fig. 2. Scale-augmented snake-like robot with 12 motors (11 joints).

3. Gait Generation

We define time-varying, continuous backbone curves to model each locomotion gait of interest in this experimental study: traveling wave rectilinear motion, lateral undulation with sinus-lifting and sidewinding. Continuous body curve representations have been applied to model many serpentine gaits that find utility in robotic systems. Planar lateral undulation[6] as well as different modes of rectilinear travel[8,39] have been modeled using this approach. Backbone curves have also been employed to model the inherently non-planar sidewinding gait.[40] For completeness, we detail the particular modeling strategy used to synthesize each gait relevant to experiments defined in Section 4 and follow-on results discussed in Section 5.

Although the traveling wave rectilinear gait is planar in nature, gait body shapes for lateral undulation with sinus-lifting and sidewinding are three-dimensional. We interpret both of the latter gaits as time-varying planar continuous body curves, in the plane of locomotion, that are then augmented with small-amplitude, vertical lift along specific segments of the body. Accordingly, each gait is decomposed into two time-varying body wave components, one defined in the horizontal plane parallel to the locomotion surface and the other defined in an orthogonal, vertical plane. Superposition of the two components then defines three-dimensional body shapes associated with lateral undulation and sidewinding.

When constructing each gait, the horizontal body wave component gets defined first. This component comprises the largest amplitude shape changes associated with both lateral undulation and sidewinding (and is trivial in the case of rectilinear motion). The smaller amplitude vertical body wave component is subsequently defined with respect to arc length along the horizontal body wave component. During the course of lateral undulation, sinus-lifting necessitates raising of body segments within which the horizontal body wave component attains peak curvature.[27] Sidewinding, on the other hand, requires vertical lift of alternating segments of vanishing curvature, along the horizontal body wave component.[18,26] Vertical lift of body segments, for both gaits, is small in amplitude and spatially dependent upon the curvature profile along the horizontal body wave component.

With the exception of the vertical body wave component of lateral undulation, we define all gait body shapes as traveling sine waves. This contrasts with standard practice, whereby gaits are modeled in curvature or joint space as time-varying sinusoidal signals, producing serpenoid body curves that accomplish each locomotion mode.[6,32,38] We find the particular geometry of the robot employed in this study, driven by off-the-shelf components, does not lend well to fine spatial resolutions needed to accomplish high-curvature gait shapes often demanded by serpenoid curves. The gait modeling approach taken here facilitates convenient dynamical models with specific applications to parallel studies.[41–44] Fitting of articulated chains to these continuous body gait models is quickly accomplished to yield commandable joint trajectories with good fit to the desired body shape.

We briefly describe the process used to compute joint trajectories for the rigid, multi-link robotic snake, from continuous body curve representations of each gait. Detailed discussion of the specific continuous body curve models used to represent each gait then follows.

3.1. Body curve fitting

A multi-link, articulated model of the robotic snake is fit to each continuous body curve gait model, at discrete instants of time over a gait cycle; joint trajectories extracted from this process define the equivalent gaits for the rigid, multi-link robot employed in follow-on experiments.

To generate joint trajectories for each gait, trajectories of joints with even IDs were first computed by fitting the discrete robot model to the time-varying horizontal body wave component. A subsequent fitting pass for the vertical component of the body wave then determined joint trajectories

https://doi.org/10.1017/S0263574718001522 Published online by Cambridge University Press

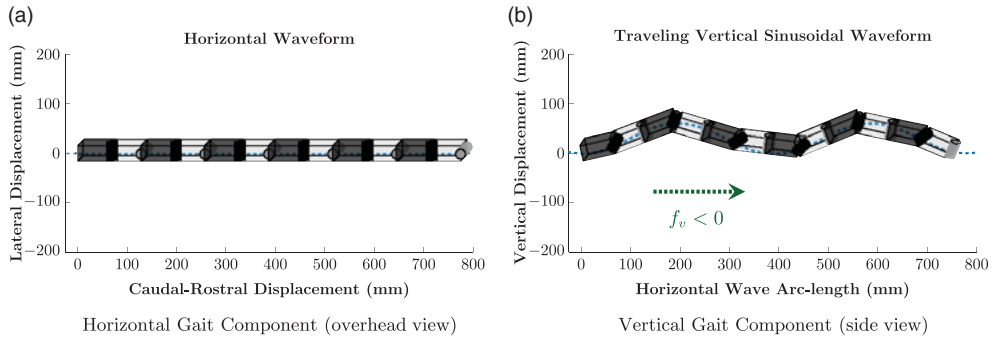

Fig. 3. Six-link robotic snake model fit to the traveling wave ***rectilinear*** gait.

associated with odd IDs. Discrete approximation of the continuous gait shapes was accomplished using a methodology similar to refs. [37,45]. For each body wave component, a forward march from the caudal to rostral ends was performed whereby the tail, each interior joint and the head were sequentially positioned coincident with the planar body wave component. Spatial link orientations and, subsequently, joint configurations were then extracted. For small amplitude variations in the vertical body wave that are characteristic of lateral undulation and sidewinding, this greedy, two-pass method worked well and was efficient.

3.2. Rectilinear motion

The rectilinear gait is defined as a rostrally traveling planar wave, inspired by gaits observed in caterpillars. Propagating a vertical sinusoidal body wave from the tail to head generates forward progression of the robotic snake.[8] Consequently, the horizontal body wave component, $y_h(x, t)$, is constrained to a straight line along an abscissa parallel to the ground plane. The vertical body wave component, $y_v(s_h, t)$, is defined to be a spatially and temporally varying sinusoid,

$$\begin{aligned} y_h(x, t) &= 0, \quad x \in [0, 2\lambda_v] \\ y_v(s_h, t) &= \frac{1}{2} A_v \left(1 - \cos\left(2\pi \left(\frac{s_h}{\lambda_v} + f_v t\right)\right)\right). \end{aligned} \tag{1}$$

Vertical wave amplitude (A_v), spatial period (λ_v) and temporal frequency (f_v) are adjustable parameters that define the rectilinear gait. The traveling body wave is illustrated in Fig. 3. The horizontal body wave component, y_h, is a straight line parametrized by x, distance along a spatial abscissa aligned with the intended direction of travel. The vertical body wave component, y_v, is the traveling sinusoid parametrized with respect to s_h, arc length along the horizontal body wave.

3.3. Lateral undulation with sinus-lifting

Sinus-lifting was incorporated into the robotic snake's lateral undulation gait. To productively employ lateral undulation, the magnitude of net rostrally directed forces must exceed counter-productive forces produced at segments of peak body curvature.[32] Sinus-lifting, as utilized by snakes, involves raising segments of peak body curvature off the locomotion surface[27] to minimize counter-productive forces.

The horizontal body wave component of the lateral undulation gait was defined by a sinusoidal traveling wave,

$$y_h(x, t) = A_h \sin\left(2\pi \left(\frac{x}{\lambda_h} + f_h t\right)\right), \quad x \in [0, \lambda_h], \tag{2}$$

where horizontal wave amplitude (A_h), wavelength (λ_h) and temporal frequency (f_h) adjust the shape of the wave. The function is parametrized with respect to distance along a spatial abscissa aligned caudal-rostrally in the intended direction of motion, x, and time, t.

To integrate sinus-lifting, local maxima in curvature along the horizontal body wave, denoted by ζ_i, are identified with respect to horizontal body wave arc length, s_h, where i indexes a particular maximum in curvature. The lateral undulation wave defined in (2) comprises a single sinusoidal

https://doi.org/10.1017/S0263574718001522 Published online by Cambridge University Press

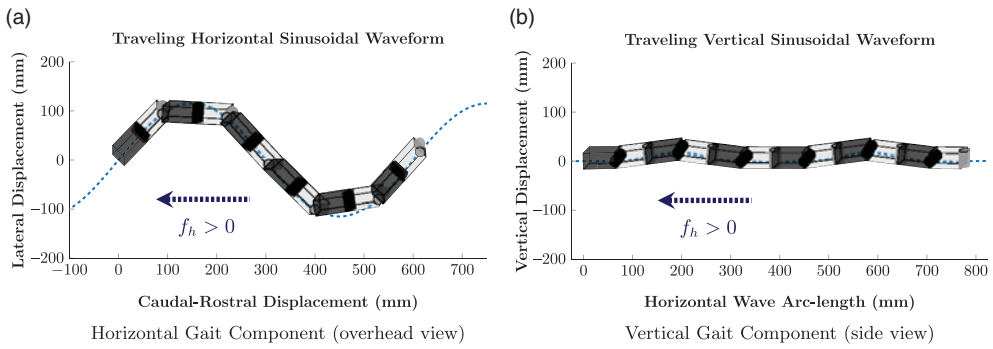

Fig. 4. Six-link robotic snake model fit to the ***lateral undulation*** gait, decomposed into horizontal and vertical body wave components.

wavelength; there are two points of peak curvature, whose arc length locations we designate by ζ_1 and ζ_2. The vertical body wave component of the gait, $y_v(s_h, t)$, is defined with respect to the horizontal body wave arc length, s_h. It is constructed by superimposing un-normalized Gaussian functions, $\gamma_i(s_h)$, each centered about a location of peak curvature, ζ_i, along the horizontal body wave. The un-normalized Gaussian function, centered about a location of peak curvature, ζ_i, takes the form

$$\gamma_i(s_h) = \exp\left(-\frac{(s_h - \zeta_i)^2}{2\sigma^2}\right), \tag{3}$$

where i indexes the particular peak in curvature being considered and ζ_i denotes the arc length location of peak i (along the horizontal body wave). Using these Gaussian bump functions, the vertical body wave, $y_v(s_h, t)$, is defined,

$$y_v(s_h) = \sum_{i=1}^{2} A_v \gamma_i(s_h). \tag{4}$$

The horizontal and vertical body wave components defining lateral undulation (with sinus-lifting) are illustrated in Fig. 4; a fit of the discrete-link robot is overlaid in each.

3.4. Sidewinding

Define the horizontal body wave component of the sidewinding gait to be the time-varying and spatially varying sinusoid,

$$y_h(x, t) = A_h \sin\left(2\pi\left(\frac{x}{\lambda_h} + f_h t\right)\right), \quad x \in [0, \lambda_h], \tag{5}$$

whose wave parameters carry the same meaning as (2). The vertical body wave component is parametrized with respect to the arc length, s_h, measured along the horizontal body wave defined in (5),

$$y_v(s_h, t) = \frac{1}{2} A_v \left(1 + \sin\left(2\pi\left(\frac{s_h}{\lambda_v} + f_v t\right) + \frac{\pi}{2}\right)\right). \tag{6}$$

The frequency of the vertical body wave, f_v, is matched to the horizontal body wave frequency, f_h. Vertical wavelength, λ_v, is assigned the total arc length measured over a single spatial period of the horizontal body wave,

$$\lambda_v = \int_0^{\lambda_h} \sqrt{1 + \left(\frac{dy_h}{dx}(x, t)\right)^2}\, dx, \tag{7}$$

https://doi.org/10.1017/S0263574718001522 Published online by Cambridge University Press

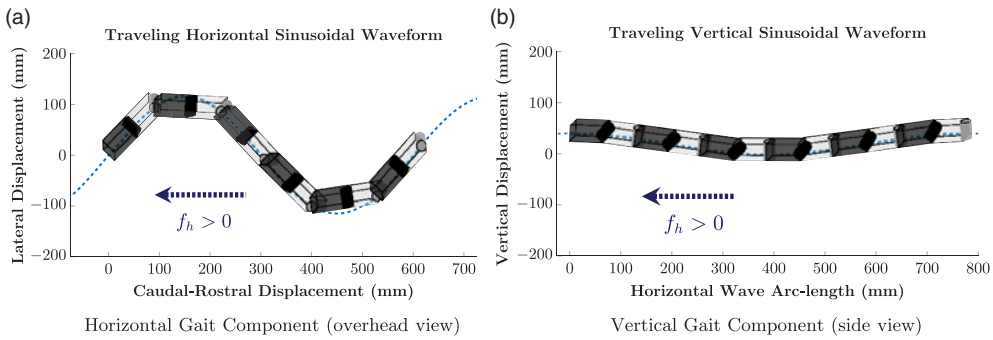

Fig. 5. Six-link robotic snake model fit to the ***sidewinding*** gait, decomposed into vertical and horizontal body wave components.

ensuring that one spatial period of the sinusoidal vertical body wave fits within one spatial period of the horizontal body wave. The three-dimensional sidewinding gait is constructed by superimposing both horizontal and vertical body wave components.

Both body wave components and a resulting fit of the robotic snake model are illustrated in Fig. 5. The phase offset of $+\frac{\pi}{2}$, in the vertical body wave (6), aligns the horizontal and vertical wave components such that segments of the horizontal body wave with a 'upward' slope, illustrated in Fig. 5, are raised vertically off the ground plane, while segments with a 'downward' slope are left un-raised and in contact with the locomotion surface.

4. Methodology

To characterize performance benefits conferred by the scaled chassis, experiments were conducted in which each of three locomotion gaits was exercised: traveling wave rectilinear motion, lateral undulation and sidewinding. Locomotion progress for each gait was measured with the artificial scales equipped as well as in their absence. Comparative analysis of the data collected was used to evaluate benefits that the scaled chassis posed for snake-like robots utilizing bio-inspired gaits described in Section 3. To evaluate the general utility of employing the artificial scales, these experiments were repeated on three distinct surface types.

4.1. Experiment

Ten experimental runs were conducted for each combination of gait (rectilinear, lateral undulation or sidewinding) and artificial scale configuration (present or absent). By arranging the uncovered, scaled side of the robot chassis to be in contact with the ground, anisotropic body–ground interactions were produced during locomotion. Two modifications were imposed to negate the effect of the scales and promote, instead, isotropic body–ground locomotive interactions. First, the robot was turned over such that the smooth (non-scaled) surface of the chassis lay against the ground. Second, the robot was inserted into a cloth tube to further promote an isotropic resistance profile with the locomotion surface. The cloth covering also mitigated effects from unintended interactions between ground asperities and chassis corners and edges. When the non-scaled chassis surface lay against the locomotion environment, absent cloth tubing, these interactions interfered with achievement of isotropic body–ground resistance profiles. Figure 2(b) and (c) depicts close-in views of the smooth chassis surface without and with the cloth tube installed, respectively.

With the exception of sidewinding, each experimental run comprised 10 cycles of a locomotion gait. In the case of sidewinding, only 4 gait cycles were executed during each experimental run in order to maintain the robot within the camera's field of view.

These experiments were repeated on each of three different surface types: carpet, inhomogeneous concrete and homogeneous concrete. Uniformly scaled images of each surface are illustrated in Fig. 6(a)–(c). An image of the scaled chassis has been juxtaposed in Fig. 6(d) to illustrate the relative size of the fabricated scales compared to the asperities that characterize each locomotion surface. The carpet surface is composed of compliant weaves that are rooted to an underlying rigid substrate. The inhomogeneous concrete surface consists of a mix of embedded smooth pebbles and large, jagged rocks. In contrast, the homogeneous concrete surface is composed of a uniform texture

https://doi.org/10.1017/S0263574718001522 Published online by Cambridge University Press

Table I. Experimental variables.

Gait	Surface	Scale Configuration
Rectilinear	Carpet	Present
Lateral undulation	Inhomogeneous concrete	Absent
Sidewinding	Homogeneous concrete	

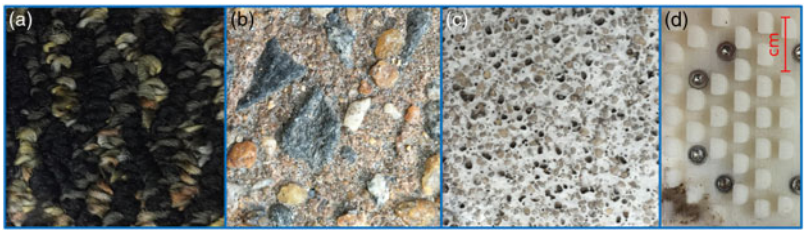

Fig. 6. Equivalent-scale comparison of surfaces employed to evaluate robot locomotive performance: (a) carpet; (b) concrete composed of large, embedded rocks of varying morphology; (c) concrete composed of uniform texture, created by smaller embedded pebbles; (d) robot chassis comprising artificial scales.

created by much smaller, evenly distributed embedded grains. All locomotion environments were previously existing surfaces; they were used to evaluate the general utility of incorporating rigid scales to enhance locomotion.

Table I depicts all experimental variables employed in this study as well as their admissible values. The set of experimental runs conducted encompasses all permutations of these variable values.

4.2. Data analysis

Locomotion progress achieved by the robot was recorded by a consumer web camera connected to a PC. White markers were placed on the scaled chassis to facilitate tracking and image processing. Additionally, the cloth tube, used to promote isotropic robot–surface interactions, was selected such that its color profile contrasted with the robot's surrounding environment.

Because the majority of experimental runs were performed outdoors, mounting the camera in an overhead position, with optical axis aligned orthogonal to the ground plane, was infeasible. A homography was instead applied to the video data to correct for any perspective skew associated with the camera's pose. After rectification of the image, background estimation was applied to the transformed video data[46] to extract the moving foreground, consisting solely of the robot in motion. Mean shift tracking, based on the robotic snake's color distribution,[47] was applied to track the effective center of mass of the robot. This collected tracking data captured the robot's trajectory during each experimental run. Principal component analysis (PCA) was subsequently applied to each measured trajectory to extract the principal direction of motion. Net displacement along this direction of travel was then computed. PCA of the robot shape was additionally extracted from the processed video, allowing measurement of net change in orientation over the course of each run.

For each scenario, defined by a particular gait and surface type, the measured net displacement and change in orientation were used to compare locomotive performance when the artificial scales were equipped versus their absence. Displacement measurements were normalized by the robot's outstretched body length and presented per gait cycle. Net change in robot orientation was measured by the angular difference between starting and ending poses, for each run.

4.3. Gait parameters

Parameter values used to construct each gait are presented in Tables II and III. Table II defines the horizontal body wave component while Table III defines the vertical body wave component, for each gait. Parameter values were selected such that desired body–ground contact patterns for each gait (described in Section 3) were accomplished and the resulting gait body shapes were satisfactorily approximated by the physical articulated robot.

https://doi.org/10.1017/S0263574718001522 Published online by Cambridge University Press

Table II. Horizontal body wave gait parameters.

Gait	A_h	f_h	λ_h
Rectilinear	0 mm	N/A	N/A
Lateral undulation	115 mm	0.2 Hz	600 mm
Sidewinding	115 mm	0.2 Hz	600 mm

Table III. Vertical body wave gait parameters.

Gait	A_v	f_v	λ_v
Rectilinear	60 mm	−0.4 Hz	390 mm
Lateral Undulation	17.5 mm	N/A	N/A
Sidewinding	40 mm	0.2 Hz	779 mm (Eq. 7)

Table IV. Displacement plot scenario labels.

Scenario Label	**Gait**	**Scale Configuration**
LU_SC	Lateral undulation	Present
LU_NS	Lateral undulation	Absent
RL_SC	Rectilinear	Present
RL_NS	Rectilinear	Absent
SW_SC	Sidewinding	Present
SW_NS	Sidewinding	Absent

Table V. Orientation plot scenario labels.

Scenario Label	**Surface**	**Scale Configuration**
CARP_SC	Carpet	Present
CARP_NS	Carpet	Absent
INHO_SC	Inhomogeneous Concrete	Present
INHO_NS	Inhomogeneous Concrete	Absent
HOM_SC	Homogeneous Concrete	Present
HOM_NS	Homogeneous Concrete	Absent

Table VI. Measured impact: net displacement (*orientation change*).

	Carpet	**Inhomogeneous concrete**	**Homogeneous concrete**
Rectilinear	+344.33% (*N/A*)	+192.53% (*N/A*)	+391.61% (*N/A*)
Lateral undulation	+97.67% (*−77.49%*)	+38.58% (*−68.77%*)	+40.39% (*−69.58%*)
Sidewinding	+1.96% (*−62.65%*)	+4.36% (*+16.22%*)	+9.62% (*−16.90%*)

5. Results

Displacement measurements collected from all experimental runs are summarized in box plots. Each box plot illustrates, for a particular surface type, discrepancies in net displacement achieved by each gait while employing the scaled chassis versus removal of the scales to facilitate isotropic robot–ground interactions. Summaries of the net change in orientation, measured for each experimental run, are also presented for the lateral undulation and sidewinding gaits. Scenario labels utilized by each box plot are defined in Tables IV and V, for displacement and orientation measurements, respectively. Impact of artificial scale presence on locomotion performance (i.e. percentage change of net displacement and orientation change) is additionally compiled in Table VI.

https://doi.org/10.1017/S0263574718001522 Published online by Cambridge University Press

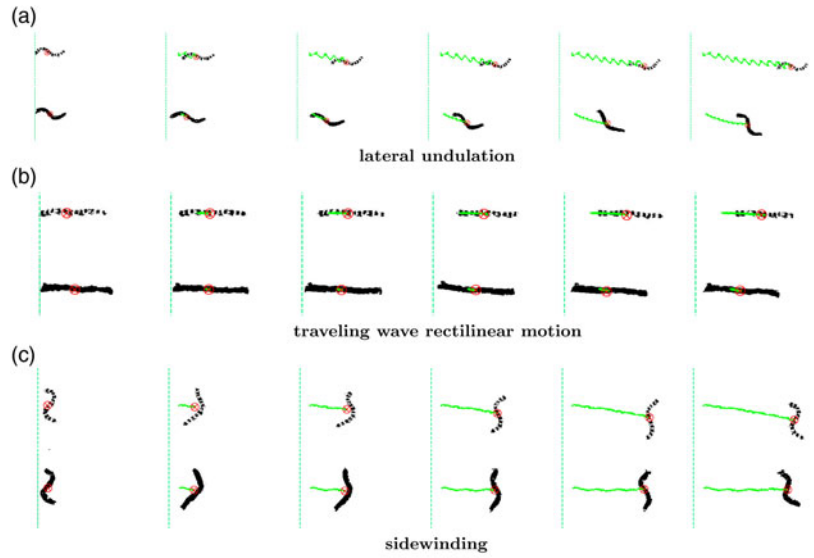

Fig. 7. Comparison of robotic snake locomotion employing each gait over the indoor ***carpet surface***. The green line illustrates the trajectory of the robot's effective center of mass. Time progresses from left to right and, within each frame, the robot additionally travels from left to right. In each sub-figure, the ***top*** sequence captures locomotion with scaled chassis equipped while the ***bottom*** sequence captures locomotion with the effect of artificial scales removed.

Representative robot trajectories, captured for each gait and surface type, are additionally illustrated in pairs of time-lapsed image sequences. The first sequence of the pair illustrates locomotion with the scaled chassis equipped while the second depicts locomotion with the effect of scales removed. They are placed side-by-side to facilitate comparison.

5.1. Carpet surface

Locomotion progress of the robot, over the carpet surface, is illustrated in Fig. 7 for each gait of interest. The top row in each sub-figure illustrates locomotion when utilizing scales, while the bottom row captures progress of the cloth-covered robotic snake. A green trajectory has been overlaid in each image sequence frame, illustrating the path traveled by the robot's effective center of mass, marked by an encircled red 'X'.

From qualitative evaluation, there is a noticeable advantage when using the scaled chassis during locomotion. Anisotropic robot–ground interactions conferred by the chassis facilitate a large increase in net displacement, particularly for the lateral undulation (Fig. 7(a)) and rectilinear (Fig. 7(b)) gaits. With respect to lateral undulation, the caudal–rostral orientation of the robot additionally remains aligned with the forward direction of travel when the scaled chassis are equipped. Without the presence of artificial scales, we find that stability of the robot heading is reduced; heading of the robot greatly deviates away from the intended direction of travel. The right-most frames of each image sequence in Fig. 7(a) illustrate this discrepancy in the robot's final orientation.

Trajectories produced by lateral undulation were consistently biased toward one lateral side of the robot. This is a consequence of the initial phasing of the gait, which was consistently reproduced at the start of every experimental run. The average body of the gait rotates asymmetrically about the horizontal centerline of the image, creating the observed trajectory bias.

In the case of the sidewinding gait, comparable progress with respect to net displacement was achieved regardless of whether artificial scales were employed. With scales equipped, however, the robot trajectory demonstrated an additional caudal-to-rostral component of displacement. This is a result that aligns with observations of sidewinders observed in nature; displacement is produced in the rostral direction, as well as laterally, resulting in a diagonal trajectory relative to the snake's caudal–rostral orientation.[48] A statistical summary of all locomotion experiments on the carpet surface is captured in Fig. 8. The box plot illustrates net displacement achieved along a straight-line path (determined by PCA), for each of the three gaits studied. Results are compared between conditions where scaled chassis were equipped and where they were removed.

https://doi.org/10.1017/S0263574718001522 Published online by Cambridge University Press

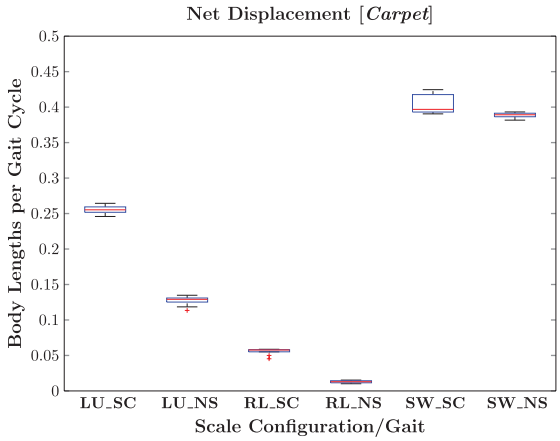

Fig. 8. **Statistical Summary**: ***Net Displacement*** produced by each gait over the ***carpet surface*** was monitored under conditions where scaled chassis were equipped versus their absence. Scenario labels are defined in Table IV.

When artificial scales were employed, the robot achieved a 97.67% increase in measured net displacement utilizing lateral undulation. This is relative to the equivalent scenario where the effect of scales was removed. A large increase in net displacement, 344.33%, was also observed for traveling wave rectilinear motion, when the scaled chassis were equipped. Sidewinding received relatively little performance enhancement from the use of scales, less than 2%.

5.2. Inhomogeneous concrete surface

To evaluate the locomotive effect of artificial scales in a different environment, the same experiments were reproduced on a concrete walkway. The structure of this surface, depicted in Fig. 6(B), is distinct from that of carpet. While the carpet surface is compliant and conforms to the shape of contacting objects, the concrete surface is rigid. It comprises a rough texture with large embedded pebbles and rocks, randomly interspersed. These larger asperities take on a variety of morphologies from smooth pebbles to large, jagged rocks. Time-lapsed image sequences capturing robot locomotion on the concrete walkway are depicted in Fig. 9. They are organized identically to those describing experimental runs on carpet (Fig. 7). Due to the presence of frequent, randomly embedded pebbles in the inhomogeneous concrete surface, a more stochastic effect was observed in the robot's trajectories over this surface, relative to the same experiments on carpet. Employing the scaled chassis clearly increased net forward displacement achieved by the robot during both lateral undulation and rectilinear motion, relative to cases where artificial scale use was proscribed. During lateral undulation, the caudal–rostral orientation of the robot additionally remained well aligned with the forward direction of travel. Similar to locomotion experiments on carpet, robot heading deviated greatly from the intended direction of travel when the effect of scales was removed. This is most evident in the right-most frames of Fig. 9(a). After 10 gait cycles of lateral undulation, without the aid of artificial scales (Fig. 9(a) bottom), net change in robot orientation approached 90 degrees clockwise. With scales equipped (Fig. 9(a) top), however, the right-most frame depicts the robot's final orientation closely aligned with its initial.

A summary of all locomotion experiments performed on the inhomogeneous concrete surface is captured in Fig. 10. The box plot is organized identically to Fig. 8, with label meanings defined in Table IV.

Lateral undulation and rectilinear motion yielded increases in the measured net displacement of 38.58% and 192.53%, respectively, when artificial scales were equipped versus their absence. Sidewinding, again, received relatively little performance benefit from utilization of scales, only a 4.36% increase in net displacement. Overall, the net forward displacement achieved by the robot, for each scenario on inhomogeneous concrete, was less than or roughly equivalent to that attained in the same scenario on carpet. However, from the standpoint of artificial scale utility, use of the scaled chassis continued to benefit locomotion.

https://doi.org/10.1017/S0263574718001522 Published online by Cambridge University Press

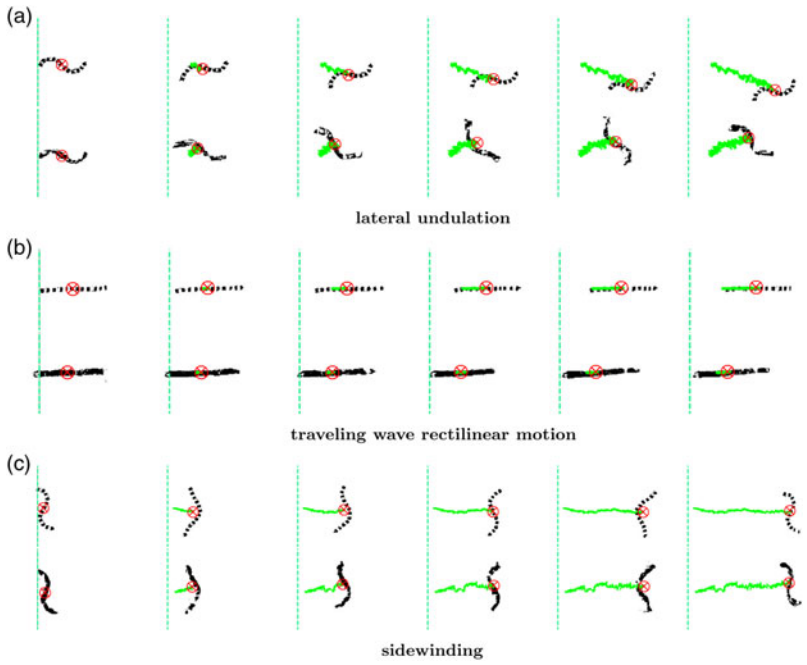

Fig. 9. Comparison of robotic snake locomotion employing each gait over the ***inhomogeneous concrete surface***. Image organization and symbology are identical to that presented in Fig. 7.

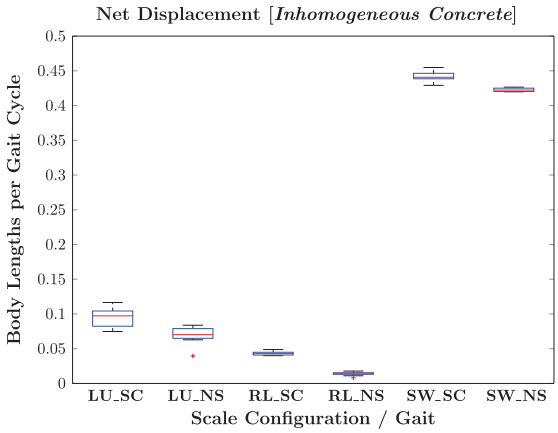

Fig. 10. **Statistical Summary**: ***Net Displacement*** produced by each gait over the ***inhomogeneous concrete surface*** was monitored under conditions where scaled chassis were equipped versus their absence. Scenario labels are defined in Table IV.

5.3. Homogeneous concrete surface

The second concrete surface on which locomotion was evaluated lacked the presence of large, randomly distributed pebbles and stones. Rather, it was composed of much smaller grains that were near-uniformly distributed over the surface. Figure 6(c) illustrates this surface's texture and the relative size of its asperities. Figure 11 depicts the time-lapsed image sequence capturing locomotion progress on this surface for each gait and is organized identically to Figs. 7 and 9.

During the course of lateral undulation, the robot's caudal–rostral orientation remained aligned with the forward direction of travel, when employing artificial scales. In the absence of scales, the robot achieved little forward displacement. Additionally, over the course of 10 gait cycles, robot orientation continually deviated further from the intended direction of travel (i.e. Fig. 11(a) left-to-right).

The right-most frames of Fig. 11(a) illustrate the final discrepancy in robot orientation when scales were employed (top) versus their absence (bottom). In the latter scenario, the final orientation of

https://doi.org/10.1017/S0263574718001522 Published online by Cambridge University Press

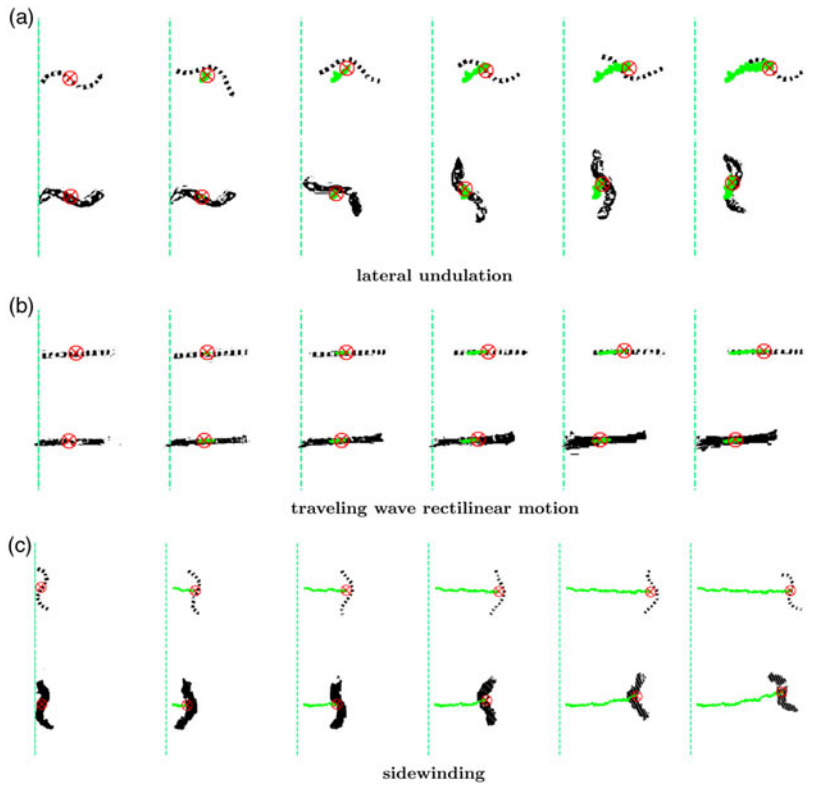

Fig. 11. Comparison of robotic snake locomotion employing each gait over the ***homogeneous concrete surface***. Image organization and symbology are identical to that presented in Figs. 7 and 9.

the robot was displaced approximately 90 degrees clockwise relative to its initial configuration; use of the scaled chassis effectively increased heading stability during the course of locomotion. The green trajectory in Fig. 11(a) (bottom) illustrates that the robot largely rotates in place in the absence of artificial scales. A statistical summary of locomotion experiments over the homogeneous concrete surface is compiled in Fig. 12, with labels defined in Table IV. With the aid of artificial scales, lateral undulation and rectilinear motion yielded increases in net displacement of 40.39% and 391.61%, respectively. We find sidewinding over homogeneous concrete also produces greater forward progress while employing the artificial scales, versus their absence, approximately 9.62%. We additionally note that the displacement achieved by lateral undulation, without use of the scaled chassis, is misleading. Direction of displacement, in this situation, deviates greatly from intended direction of travel (i.e. left-to-right in Fig. 11(a)); after a large amount of rotation, the robot travels in the wrong direction.

With respect to scaled locomotion across all surface types, travel distance on the homogeneous concrete surface, for each gait, was less than or roughly equivalent to that measured on the inhomogeneous concrete and carpet surfaces.

5.4. Heading stability

The net change in orientation, measured between starting and ending configurations of the robot in each experimental run, is summarized in Figs. 13 and 14 for lateral undulation and sidewinding scenarios, respectively.

Figure 13 quantitatively characterizes heading stability of the robot when executing lateral undulation. It complements previous qualitative observations and captures a statistical summary of the net change in heading, measured over all recorded scenarios. With the anisotropic robot–ground forcing profile conferred by the equipped scaled chassis, the robot was better able to maintain its heading over each surface type in contrast to scenarios where effect of the artificial scales was removed. Over the course of 10 gait cycles of lateral undulation, the median measured deviation in orientation was reduced to 77.49%, 68.77% and 69.58% on the carpet, inhomogeneous concrete and homogeneous

https://doi.org/10.1017/S0263574718001522 Published online by Cambridge University Press

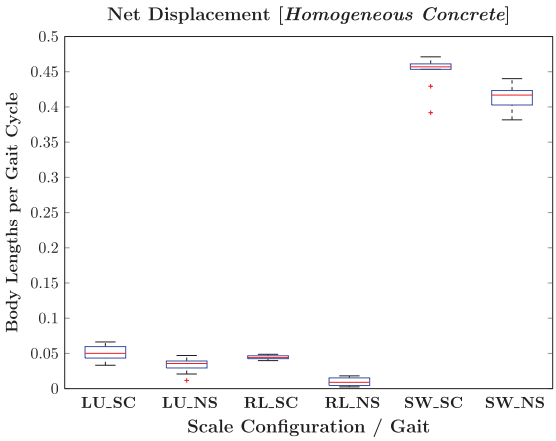

Fig. 12. **Statistical Summary**: ***Net Displacement*** produced by each gait over the ***homogeneous concrete surface*** was monitored under conditions where scaled chassis were equipped versus their absence. Scenario labels are defined in Table IV.

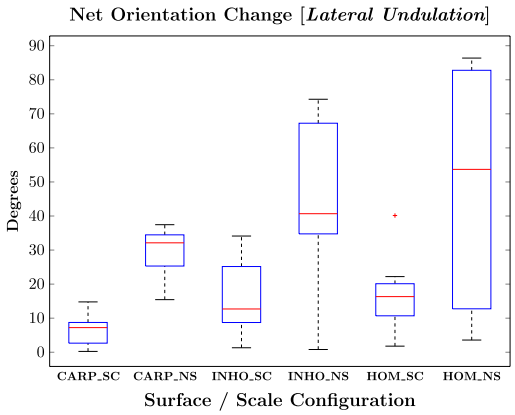

Fig. 13. **Statistical Summary**: ***Net orientation change*** produced by ***lateral undulation*** was measured during each experimental run. Results are organized according to labels defined in Table V.

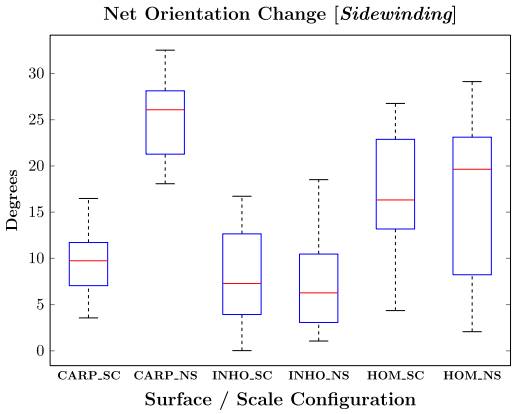

Fig. 14. **Statistical Summary**: ***Net orientation change*** generated by ***sidewinding*** was measured during each experimental run. Results are organized according to labels defined in Table V.

concrete surfaces, respectively. Tighter variance was also observed in these measured heading deviations when artificial scales were equipped to the robotic snake, as opposed to their absence. This smaller variance in the measured net orientation change of the robot is especially salient on the concrete surfaces.

https://doi.org/10.1017/S0263574718001522 Published online by Cambridge University Press

In contrast, the sidewinding gait received no notable benefit with respect to heading stability on either of the concrete surface types. Measured performance, depicted in Fig. 14, was comparable with and without the scaled chassis equipped on these surfaces. With respect to the carpet surface, however, a 62.65% reduction in heading deviation was measured.

6. Discussion

Each surface type employed in these experiments induced different robot–ground interactions that impacted the effectiveness of the scaled chassis. Based on experimental results, comparison of locomotive performance across different surface types, for each gait, is discussed.

6.1. Traveling wave rectilinear motion

Comparable net displacements were produced on each surface type using the traveling wave rectilinear gait. When scaled chassis were equipped, average measured displacements were 0.0555, 0.0434 and 0.0444 body lengths per gait cycle on carpet, inhomogeneous concrete and homogeneous concrete surfaces, respectively. These values remained greater, however, than equivalent scenarios where the effect of the artificial scales was removed (0.0129, 0.0142 and 0.0098 body lengths per gait cycle, respectively); the scaled chassis, and accompanying anisotropic robot–ground interactions, enhanced locomotive performance on each surface type, relative to its absence.

Two additional observations are noted. The low variance in net displacement measured across all surface types, when the scaled chassis were equipped, suggests that the rectilinear locomotive mode of travel may not rely on the presence of environmental forcing as critically as, for example, lateral undulation. Yet, the discrepancies between locomotive performance with and without use of artificial scales indicate that caudal–rostral anisotropic environmental forcing is still important. These two observations lead us to conjecture that the effective caudal-to-rostral friction ratio is important for predicting rectilinear robotic snake locomotion. We are currently working on modeling the dynamics of rectilinear movement to explore this conjecture.[41,42]

6.2. Lateral undulation

The lateral undulation gait was selected for these experiments due to its dependence, in nature, on directionally dependent body–ground forcing. An anisotropic friction profile between the snake ventral surface and locomotion environment is understood to be an important component of productive gait execution in nature.[27] The magnitude of frictional resistance applied by the environment differs depending on the direction of relative velocity between the snake venter and locomotion surface. Equipping a robotic snake with artificial scales was expected to enhance its locomotive performance when employing this gait. The scaled chassis were designed to generate relatively large robot–ground resistive forcing when translating laterally, in an effort to reduce transverse slip. Improvements in locomotive performance, when the scaled chassis were equipped, are evident in experimental results presented in Section 5.

Integrating the artificial scales into the robot resulted in increases in forward displacement relative to conditions where the fabricated scales were absent. Lateral undulation employing artificial scales produced the largest gains on the carpet surface, 97.67%, followed by gains of 38.58% on the inhomogeneous concrete surface and 40.39% on the homogeneous concrete surface. The latter gain is additionally coupled with a consistent observation that the robotic snake, without scales, made little progress in the intended direction of travel, largely rotating in place. Equipping the scaled chassis additionally aided stabilization of the robot's heading, over the course of gait execution. Removal of the scaled chassis resulted in heading deviations away from a straight-line path. Figure 13 illustrates how this deviation worsened as the surface type changed from carpet to inhomogeneous concrete, becoming worst on homogeneous concrete. With the scaled chassis equipped, the heading remained relatively stable on each surface type; median orientation deviations were reduced by more than 68%.

Examination of net displacement across all surface types, with the scaled chassis equipped, reveals large discrepancies. Ten gait cycles of lateral undulation executed on the carpet surface resulted in median forward displacement of 2.55 body lengths. By comparison, lateral undulation on inhomogeneous concrete and homogeneous concrete surfaces only resulted in displacements of 0.97 and 0.50 body lengths, respectively. Gait performance, with respect to the robot's net displacement, exhibited a dependence on robot–ground interactions specific to each surface.

https://doi.org/10.1017/S0263574718001522 Published online by Cambridge University Press

6.3. Sidewinding

Net displacement generated by the sidewinding gait was impacted relatively little from equipping the scaled chassis versus their absence. Gait execution employing the artificial scales resulted in performance increases of 1.96%, 4.36% and 9.62% across carpet, inhomogeneous concrete and homogeneous concrete surfaces, respectively. With respect to heading stability, the fabricated scales conferred no notable advantage on either concrete surface but did produce a distinguishable benefit on carpet, reducing deviations in heading as well as narrowing the associated variance. Despite a lesser impact to sidewinding performance overall, however, no appreciably detrimental outcomes were measured when artificial scales were equipped.

These results suggest that utilization of the scaled chassis and furthermore anisotropic body–ground forcing may not have great utility for all modes of snake-like locomotion. Sidewinding, in particular, is a locomotion mode exhibited by a species of viper inhabiting desert environments where the ground substrate has high tendency to yield. The gait, as observed in nature, is understood to rely predominantly on static contact between the body ventral surface and locomotion medium.[18,48,49] The 'pick-up and place' step-like motion, entailed in sidewinding, minimizes slip and curtails the relevance of sliding friction during locomotion. Accordingly, we observe that the forward displacement achieved by the robot was largely invariant to both scale presence as well as surface type; the step-like motion pattern characterizing this gait facilitated locomotive performance predominantly independent of body–ground friction properties.

7. Conclusion and Future Work

This study evaluated the locomotive performance enhancements conferred by mounting biologically inspired scales to the ventral surface of a robotic snake, promoting anisotropic body–ground interactions with the locomotion surface. Doing so involved design, fabrication and experimental evaluation of a robot chassis with integrated 3-D printed scales that promote directionally dependent resistance between the robot body and non-smooth locomotion surfaces. Performance, with the scaled chassis equipped as well as with the effect of artificial scales removed, was examined for three different modes of locomotion: traveling wave rectilinear motion, lateral undulation and sidewinding. All gaits were additionally evaluated on each of three distinct surface types: carpet, inhomogeneous concrete and homogeneous concrete.

Integration of the fabricated scales into the robot chassis was found to enhance locomotive performance for each gait exercised. The greatest improvements to net displacement were measured for lateral undulation and rectilinear motion, gaits for which directional friction is a recognized factor impacting motion in the robot's biological counterparts. Gait performance improved regardless of the surface type employed. Positive, though smaller, gains were measured for the sidewinding gait.

Use of the scaled chassis was additionally observed to stabilize robot heading, particularly in the case of lateral undulation. Net change in robot orientation, measured during this gait, greatly decreased when artificial scales were equipped to the robot. Variance associated with this measurement additionally remained tight in scenarios where the scaled chassis were equipped, relative to their absence.

The results presented demonstrate that performance associated with several useful and widely applied modes of snake-like locomotion benefit from the bio-inspired, scaled chassis. By integrating artificial scales into their bodies, many other platforms belonging to this class of mobile robotic systems may potentially gain similar locomotive benefits. Ultimately, employment of this bio-inspired mechanism facilitates greater competency when traversing non-smooth, flat terrain of a variety of characterizations, both broadening and enhancing the general utility of elongated-body mobile robots.

Parallel efforts focus on the derivation of dynamical models for each gait.[42,43] Locomotion outcomes under different frictional ratios for these dynamical models will provide quantitative outcomes with respect to the effect of frictional anisotropy and potentially optimal configurations per gait. When coupled with experiment, these models are expected to facilitate estimation of the actual frictional properties characterizing each locomotion environment and, ultimately, motion planning and traversal through arbitrary scenarios situated in those environments.[41,44]

Acknowledgments

This work was supported by the National Science Foundation (NSF Award #1562911).

References

1. H. Maruyama and K. Ito, "Semi-autonomous snake-like robot for search and rescue," *IEEE Safety Security and Rescue Robotics*, Bremen, Germany (July 2010) pp. 1–6.
2. A. Ferworn, C. Wright, J. Tran, C. Li and H. Choset, "Dog and Snake Marsupial Cooperation for Urban Search and Rescue Deployment," *IEEE International Symposium on Safety, Security, and Rescue Robotics*, College Station, TX (November 2012) pp. 1–5.
3. A. R. Ansari, J. Whitman, B. Saund and H. Choset, "Modular platforms for advanced inspection, locomotion, and manipulation," *43rd Annual Waste Management Conference*, Phoenix, AZ (March 2017) pp. 1–11.
4. J. Whitman, N. Zevallos, M. Travers and H. Choset, "Snake robot urban search after the 2017 mexico city earthquake," *IEEE International Symposium on Safety, Security, and Rescue Robotics*, Philadelphia, PA (August 2018) pp. 1–6.
5. R. R. Murphy, S. Tadokoro, D. Nardi, A. Jacoff, P. Fiorini, H. Choset, and A. M. Erkmen, "Search and Rescue Robotics," **In**: *Springer Handbook of Robotics* (B. Siciliano and O. Khatib, eds.) (Springer-Verlag, Berlin, Heidelberg, 2008) ch. 50, pp. 1151–1174.
6. S. Hirose, *Biologically Inspired Robots: Snake-Like Locomotors and Manipulators* (Oxford Science Publications, Oxford, 1987).
7. M. Mori and S. Hirose, "Development of Active Cord Mechanism ACM-R3 with Agile 3D Mobility," *IEEE International Conference on Intelligent Robots and Systems*, Maui, HI (October 2001) pp. 1552–1557.
8. G. Chirikjian and J. Burdick, "The kinematics of hyper-redundant robot locomotion," *IEEE Trans. Rob. Autom.* **11**(6), 781–793 (1995).
9. H. Kimura and S. Hirose, "Development of Genbu: Active Wheel Passive Joint Articulated Mobile Robot," *IEEE International Conference on Intelligent Robots and Systems*, Lausanne, Switzerland (2002) pp. 823–828.
10. J. Borenstein, G. Granosik and M. Hansen, "The OmniTread Serpentine Robot—Design and Field Performance," *Proceedings of the SPIE Defense and Security Conference, Unmanned Ground Vehicle Technology VII*, Orlando, FL (2005) pp. 324–332.
11. T. Kamegawa, T. Yamas, H. Igarashit and F. Matsunos, "Development of the Snake-like Rescue Robot 'KOHGA'," *IEEE International Conference on Robotics and Automation*, New Orleans, LA (2004) pp. 5081–5086.
12. C. Wright, A. Buchan, B. Brown, J. Geist, M. Schwerin, D. Rollinson, M. Tesch and H. Choset, "Design and Architecture of the Unified Modular Snake Robot," *IEEE International Conference on Robotics and Automation*, Saint Paul, MN (2012) pp. 4347–4354.
13. W. Zhen, C. Gong and H. Choset, "Modeling Rolling Gaits of A Snake Robot," *IEEE International Conference on Robotics and Automation*, Seattle, WA (2015) pp. 3741–3746.
14. D. Rollinson and H. Choset, "Gait-Based Compliant Control for Snake Robots," *IEEE International Conference on Robotics and Automation*, Karlsruhe, Germany (2013) pp. 5123–5128.
15. A. A. Transeth, R. I. Leine, C. Glocker and K. Y. Pettersen, "Non-smooth 3D Modeling of a Snake Robot with External Obstacles," *IEEE International Conference on Robotics and Biomimetics*, vol. 7491, Kunming, China (2006), pp. 1189–1196.
16. A. A. Transeth, R. I. Leine, C. Glocker, K. Y. Pettersen and S. Member, "Snake robot obstacle-aided locomotion: Modeling, simulation, and experiments," *IEEE Trans. Robot.* **24**(1), 88–104 (2008).
17. P. Liljeback, K. Pettersen, O. Stavdahl and J. Gravdahl, "Experimental investigation of obstacle-aided locomotion with a snake robot," *IEEE Trans. Robot.* **27**(4), 792–800 (2011).
18. J. Gray, "The mechanism of locomotion in snakes," *J. Exp. Biol.* **23**(2), 101–120 (1946).
19. F. Sanfilippo, J. Azpiazu, G. Marafioti, A. A. Transeth, Ø. Stavdahl and P. Liljebäck, "Perception-driven obstacle-aided locomotion for snake robots: The state of the art, challenges and possibilities," *Appl. Sci.* **7**(4) (2017).
20. F. Sanfilippo, Ø. Stavdahl and P. Liljebäck, "SnakeSIM: A ROS-based Rapid-prototyping Framework for Perception-driven Obstacle-aided Locomotion of Snake Robots," *IEEE International Conference on Robotics and Biomimetics* (2017) pp. 1226–1231.
21. P. Liljebäck, K. Y. Pettersen, Ø. Stavdahl and J. T. Gravdahl, "Compliant Control of the Body Shape of Snake Robots," *IEEE International Conference on Robotics and Automation* (2014) pp. 4548–4555.
22. M. J. Travers, J. Whitman, P. E. Schiebel, D. I. Goldman and H. Choset, "Shape-based Compliance in Locomotion," *Robotics: Science and Systems*, Ann Arbor, MI (June 2016).
23. C. Gong, M. Travers, X. Fu and H. Choset, "Extended Gait Equation for Sidewinding," *IEEE International Conference on Robotics and Automation*, Sacramento, CA (2013) pp. 5162–5167.
24. R. Hatton, R. Knepper, H. Choset, D. Rollinson, C. Gong and E. Galceran, "Snakes on a Plan: Toward Combining Planning and Control," *IEEE International Conference on Robotics and Automation*, Karlsruhe, Germany (2013) pp. 5174–5181.
25. X. Xiao, E. Cappo, W. Zhen, J. Dai, K. Sun, C. Gong, M. Travers and H. Choset, "Locomotive Reduction for Snake Robots," *IEEE International Conference on Robotics and Automation*, Seattle, WA (2015) pp. 3735–3740.
26. H. C. Astley, C. Gong, J. Dai, M. Travers, M. M. Serrano, P. A. Vela, H. Choset, J. R. Mendelson, D. L. Hu and D. I. Goldman, "Modulation of orthogonal body waves enables high maneuverability in sidewinding locomotion," *Proc. Natl. Acad. Sci. USA* **112**(19), 6200–6205 (2015).
27. D. L. Hu, J. Nirody, T. Scott and M. J. Shelley, "The mechanics of slithering locomotion," *Proc. Natl. Acad. Sci. USA* **106**(25), 10081–10085 (2009).

28. J. Hazel, M. Stoneb, M. Gracec and V. Tsukruk, "Nanoscale design of snake skin for reptation locomotions via friction anisotropy," *J . Biomech.* **32**(5), 477–484 (1999).
29. R. A. Berth, G. Westhoff, H. Bleckmann and S. N. Gorb, "Surface structure and frictional properties of the skin of the Amazon tree boa Corallus hortulanus (Squamata, Boidae)," *J. Comp. Physiol. A* **195**, 311–318 (2009).
30. A. Filippov and S. N. Gorba, "Frictional-anisotropy-based systems in biology: Structural diversity and numerical model," *Sci. Rep.* **3**(1240) (2013).
31. H. Marvi, J. Cook, J. Streator and D. Hu, "Snakes move their scales to increase friction," *Biotribology* **5**, 52–60 (2016).
32. P. Liljeback, K. Pettersen, O. Stavdahl and J. Gravdahl, *Snake Robots: Modelling, Mechatronics, and Control* (Springer-Verlag, London, 2013).
33. M. Saito, M. Fukuya and T. Iwasaki, "Serpentine locomotion with robotic snakes," *IEEE Control Syst. Mag.* **22**(1), 64–81 (2002).
34. J. Hopkins and S. Gupta, "Design and modeling of a new drive system and exaggerated rectilinear-gait for a snake-inspired robot," *J. Mech. Robot.* **6**(2), 021001–021008 (2014).
35. W. Wang and S. Wu, "A caterpillar climbing robot with spine claws and compliant structural modules," *Robotica* **34**, 1553–1565 (2016).
36. P. Manoonpong, D. Petersen, A. Kovalev, F. Wörgötter, S. N. Gorb, S. Marlene and L. Heepe, "Enhanced locomotion efficiency of a bio-inspired walking robot using contact surfaces with frictional anisotropy," *Sci. Rep.* **6**(39455) (2016).
37. M. Serrano, A. Chang, G. Zhang and P. Vela, "Incorporating Frictional Anisotropy in the Design of a Robotic Snake through the Exploitation of Scales," *IEEE International Conference on Robotics and Automation*, Seattle, WA (2015) pp. 3729–3734.
38. M. Tesch, K. Lipkin, I. Brown, R. Hatton, A. Peck, J. Rembisz and H. Choset, "Parameterized and scripted gaits for modular snake robots," *Adv. Robot.* **23**(9), 1131–1158 (2012).
39. G. S. Chirikjian and J. W. Burdick, "Kinematics of Hyper-redundant Robot Locomotion with Applications to Grasping," *IEEE International Conference on Robotics and Automation*, Sacramento, CA (1991) pp. 720–725.
40. J. Burdick, J. Radford and G. Chirikjian, "A 'Sidewinding' Locomotion Gait for Hyper-redundant Robots," *IEEE International Conference on Robotics and Automation*, vol. 3, Atlanta, GA (1993) pp. 101–106.
41. A. Chang and P. Vela, "Closed-loop Path Following of Traveling Wave Rectilinear Motion through Obstacle-strewn Terrain," *IEEE International Conference on Robotics and Automation*, Singapore (2017) pp. 3532–3537.
42. A. Chang, M. Serrano and P. Vela, "Shape-centric Modeling of Traveling Wave Rectilinear Locomotion for Snake-like Robots," *IEEE Conference on Decision and Control*, Las Vegas, NV (2016) pp. 7535–7541.
43. A. Chang, M. Serrano and P. Vela, "Shape-centric Modeling of Lateral Undulation and Sidewinding Gaits for Snake Robots," *IEEE Conference on Decision and Control*, Las Vegas, NV (2016) pp. 6676–6682.
44. A. Chang, N. Hyun, E. Verriest and P. Vela, "Optimal Trajectory Planning and Feedback Control of Lateral Undulation in Snake-Like Robots," *Proceedings of the American Control Conference*, Milwaukee, WI (2018) pp. 2114–2120.
45. S. B. Andersson, "Discrete Approximations to Continuous Curves," *IEEE International Conference on Robotics and Automation*, Orlando, FL (2006) pp. 2546–2551.
46. V. Reddy, C. Sanderson and B. C. Lovell, "An Efficient and Robust Sequential Algorithm for Background Estimation in Video Surveillance," *IEEE International Conference on Image Processing*, Cairo, Egypt (2009) pp. 1109–1112.
47. D. Comaniciu, V. Ramesh and P. Meer, "Real-time Tracking of Non-rigid Objects Using Mean Shift," *IEEE Conference on Computer Vision and Pattern Recognition*, vol. 2, Hilton Head Island, SC (2000) pp. 142–149.
48. W. Mosauer, "On the locomotion of snakes," *Science* **76**(1982), 583–585 (1932).
49. H. Marvi, C. Gong, N. Gravish, H. Astley, M. Travers, R. L. Hatton, J. R. Mendelson III, H. Choset, D. L. Hu and D. I. Goldman, "Sidewinding with minimal slip: Snake and robot ascent of sandy slopes," *Science* **346**, 224–229 (2014).

https://doi.org/10.1017/S0263574718001522 Published online by Cambridge University Press